crystals

MDPI

Article

Electronic Structure of Oxygen-Deficient $SrTiO_3$ and Sr_2TiO_4

Ali Al-Zubi, Gustav Bihlmayer * and Stefan Blügel

Peter Grünberg Institut (PGI-1) and Institute for Advanced Simulation (IAS-1), Forschungszentrum Jülich and JARA, 52428 Jülich, Germany

* Correspondence: g.bihlmayer@fz-juelich.de

Received: 18 October 2019; Accepted: 1 November 2019; Published: 7 November 2019

Abstract: The conductive behavior of the perovskite $SrTiO_3$ is strongly influenced by the presence of oxygen vacancies in this material, therefore the identification of such defects with spectroscopic methods is of high importance. We use density functional theory to characterize the defect-induced states in $SrTiO_3$ and Sr_2TiO_4. Their signatures at the surface, the visibility for scanning tunneling spectroscopy and locally conductive atomic force microscopy, and the core-level shifts observed on Ti atoms in the vicinity of the defect are studied. In particular, we find that the exact location of the defect state (e.g., in SrO or TiO_2 planes relative to the surface) are decisive for their visibility for scanning-probe methods. Moreover, the usual distinction between Ti^{3+} and Ti^{2+} species, which can occur near defects or their aggregates, cannot be directly translated in characteristic shifts of the core levels. The width of the defect-induced in-gap states is found to depend critically on the arrangement of the defects. This also has consequences for the spectroscopic signatures observed in so-called resistive switching phenomena.

Keywords: perovskite oxides; defect states; density functional theory

1. Introduction

The electronic properties of many insulating oxides, such as $SrTiO_3$, are strongly determined by defects, in particular (but not exclusively) oxygen vacancies. Probably the most dramatic evidence for this influence can be seen in the phenomenon of resistive switching where a voltage pulse, smaller than the band gap of the material, leads to electric conductance [1–4]. While different models have been proposed that aim at an explanation of this behavior (e.g., [5–7]), they all agree in the fact that some region of increased deviations from stoichiometry in the material is necessary to enable the observed conductivity, separated by a more or less insulating matrix. One could assume that the question how and under which condition such an increased concentration of defects is likely to form can easily be addressed by ab initio theory. Indeed, several studies based on density functional theory (DFT) have investigated this problem and, rather counter-intuitively, under certain conditions tendencies for vacancy clustering were found [8,9]. This behavior is not unknown in other oxides, e.g., TiO_2, where it is actually well accepted that extended defects act as precursor phases for the formation of Magnèli phases such as Ti_5O_9 or Ti_4O_7 [10,11]. DFT calculations indeed find that such tendencies towards linear ordering of defects exist and relate that to observed resistive switching phenomena [12].

Next to the question of energetics, i.e., whether and under which condition vacancy ordering is favorable, another important aspect concerns the impact of these vacancy arrangements on the electronic structure. While an isolated defect forms a shallow donor state near the conduction band, extended

defects can give rise to band-like features in the band gap [4]. However, also near surfaces or otherwise electronically inactive stacking faults, e.g., in SrO-rich Ruddlesden–Popper phases, the electronic properties of oxygen vacancies can vary considerably depending on their position and arrangement. Even though it is presently possible to map out Ti^{3+} and Ti^{4+} by the combination of atomic-resolution imaging and spectroscopic methods [13], it is difficult to relate the spectra to the precise chemical environment of the observed species. Moreover, the detection limit of a method like X-ray photoelectron spectroscopy is usually limited (among other factors) by the peak separation of the species (e.g., in rutile TiO_2 a limit of 0.5% was assumed for the Ti^{4+}/Ti^{3+} ratio [14]). Therefore, the knowledge of the expected peak positions can help in the deconvolution of the spectra. In our study, we want to address these questions based on DFT calculations that help to interpret experimental findings, e.g., by relating them to spectroscopic signatures that can be obtained from the inner regions of a defective crystal.

Various *ab initio* calculations were performed to study the bulk properties and the electronic structure of cubic perovskite phases [15–17]. Formation energies of a single O-vacancy in bulk $SrTiO_3$ were analyzed using different DFT exchange-correlation functionals and different super cell sizes [18–21]. It was realized that the DFT band gap underestimation can severely affect the energetics of the vacancy states inside the gap. All these previous DFT calculations showed that the formation energy of neutral single O-vacancy decreases with increasing super cell size, i.e., low defect concentration is favorable in the $SrTiO_3$ bulk. Asta et al. calculated lower formation energies for singly and doubly positively charged vacancies, compared to the neutral species [22]. Samanta et al. analyzed the stability of O-vacancies and interstitials in their different charge states. They found that at low oxygen partial pressure, neutral O-vacancies are most dominant. On the other hand, doubly charged oxygen vacancies (V_O^{2+}) are dominant at intermediate and high oxygen partial pressure [23]. A recent study, combining DFT and model Hamiltonians, found that the oxygen vacancy-induced localized state is highly one-dimensional and is mainly composed of Ti $3d_{z^2-r^2}$ orbitals, and that the oxygen vacancy does not lead to Ti t_{2g}-based localized states [24]. By studying the electron correlation effects, it was concluded that oxygen vacancies in $SrTiO_3$ can produce a deep in-gap level state in photoemission spectroscopy [25]. Using DFT+U calculations, polarons could be stabilized near oxygen vacancies giving rise to states between 0.8 and 1.1 eV below the conduction band [26]. Given this variety of findings, establishing firm relations between experimental signatures and a microscopic picture is again of prime importance.

First, we will explore the electronic properties of individual defects in the bulk and at or near the (001) surfaces of $SrTiO_3$, investigating their visibility for scanning tunneling microscopy and core-level spectroscopies. Then we focus at linearly arranged oxygen vacancies in the bulk of $SrTiO_3$, identifying again strong geometrical effects. Finally, similar observations can be made in Ruddlesden–Popper phases.

2. Results

2.1. Bulk and Surface of $SrTiO_3$

2.1.1. Isolated Defects

Our calculations using a $2 \times 2 \times 4$ bulk unit cell show a narrow defect state with 0.12 eV bandwidth located 0.19 eV below the conduction band minimum. Note that we consider an overall charge neutral system without the formation of polarons [27]. As mentioned above, depending on the calculational model, DFT calculations and their extensions (DFT+U, hybrid functionals) can lead to different descriptions of the defect state [28]. In our model, the two electrons that are left behind near the vacancy distribute evenly between the two neighboring Ti atoms forming orbitals of $d_{z^2-r^2}$ shape. Although it is tempting to associate these Ti atoms with a formal charge $+1$, the analysis of the charge density shows that within a sphere of 2 Å diameter the local charge is increased by only 0.05 d-electrons as compared to Ti sites far

from the vacancy. The shift of the $2p_{1/2}$ (1*s*) core levels of these atoms amounts to 0.63 eV (0.53 eV) to lower binding energies, i.e., smaller than expected for nominal Ti^{3+} but larger than anticipated from the small increase of charge [29]. E.g. in $LaAlO_3/SrTiO_3$ heterostructures, where the presence of Ti^{3+} is expected at the interfaces, binding energy shifts of about 1.5 eV were found in X-ray photoelectron spectroscopy [30].

Recent scanning tunneling spectroscopy experiments on SrO and TiO_2 terminated $SrTiO_3$ (001) surfaces found signatures of defect states created by oxygen vacancies at the SrO terminated surface, while no such signals were observed at TiO_2 terminated ones [31]. On the SrO terminated surface, an oxygen defect has only a single Ti nearest neighbor and formally, this could be labeled as Ti^{2+} species. Nevertheless, our calculation gives only a moderate shift of the $2p_{1/2}$ core level of 0.60 eV. This can be attributed to a strong inwards relaxation of the nearest-neighbor Ti atom resulting in a strongly decreased distance to the oxygen atom directly below it. On the other hand, next-nearest-neighbor Ti atoms that show smaller relaxations show slightly higher core-level shifts (0.70 eV).

At finite temperatures there might be the possibility that oxygen vacancies migrate from the surface to deeper layers or a small but finite oxygen partial pressure leads to a filling of the surface defects. But even if the oxygen vacancy is located not directly in the surface layer but in the next SrO layer underneath the surface, there should be visible traces of the defect state at the surface. In Figure 1 we show the density of states and the charge density profiles of the neutral defect state that is located at the conduction band minimum. At the position of the surface oxygen atoms we observe a square-like charge density profile with its corners oriented towards the neighboring Sr atoms.

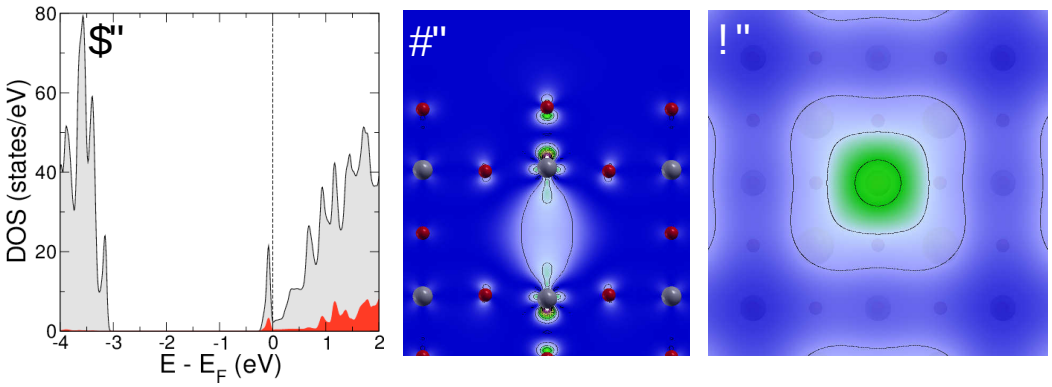

Figure 1. Electronic structure of a sub sub-surface oxygen vacancy at the SrO terminated (001) surface of $SrTiO_3$: (**a**) Density of states (DOS) around the Fermi level: the total DOS is shown in gray, the local DOS at the Ti atoms adjacent to the vacancy in red. (**b**) Charge density associated with the shallow in-gap state at the conduction band edge shown in panel (a). The cut is taken in the (100) plane. Red (gray) circles indicate oxygen (titanium) atoms. (**c**) Charge density of the same state in a (001) plane 2.4 Å above the surface. In the calculations, a $p(2 \times 2)$ unit cell was assumed.

For oxygen vacancies in the TiO_2 planes we assumed a $(\sqrt{5} \times \sqrt{5})$ unit cell following the periodicity observed with scanning tunneling microscopy measurements of the TiO_2 terminated surface by Tanaka et al. [32]. DFT+U calculations for oxygen defects at the surface have been performed e.g., by Fang and Terakura [33] who found a spin-polarized split-off state in the gap, while another DFT study used hybrid functionals found a nonmagnetic defect level in the TiO_2-terminated surface [21]. Yet another DFT study found a significant surface reconstruction after introducing oxygen vacancies [34]. The different charge density distributions at the two different surfaces were shown in Ref. [31], where it was argued that the in-plane orientation of the defect states could be responsible for the fact that the defects are not visible at the TiO_2 terminated (001) surface.

In Figure 2 we analyze again the case when the defects are not directly in the surface plane but in the next TiO_2 plane below the surface. Note that the apparent reduction of the band gap in panel (a) is caused by states from the topmost TiO_2 layer at the valence band maximum [35]. These states have only a small effect on the position of the defect states located at the conduction band minimum. A cut through the (001) plane containing the defect position is shown in Figure 2b. The charge density located above the surface is plotted in panel (c) in the same color scheme as Figure 1c. The pattern observed on the surface shows some similarity to scanning tunneling microscopy images observed on TiO_2 terminated surfaces [36]. Also here, the shift of the $2p_{1/2}$ core level is small and amounts to 0.27 eV, which is even smaller than what we found for bulk defects.

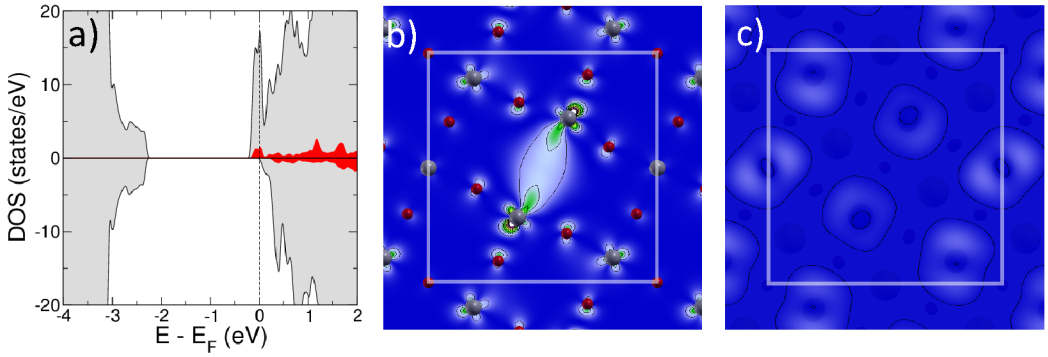

Figure 2. Electronic structure of a sub sub-surface oxygen vacancy at the TiO_2 terminated (001) surface of $SrTiO_3$: (**a**) Density of states (DOS) around the Fermi level, the majority (minority) spin DOS is shown as positive (negative) numbers. Like in Figure 1, the total DOS is shown in gray, the local DOS at the Ti atoms adjacent to the vacancy in red. (**b**) Charge density associated with the defect state below the Fermi level in a (001) plane including the vacancy. The $(\sqrt{5} \times \sqrt{5})$ unit cell is outlined in gray, the color code of the atoms follows Figure 1. The in-plane orientation of the defect states is clearly visible. (**c**) Charge density of the defect state in a (001) plane 2.4 Å above the surface with the same coloring scheme as in Figure 1c.

2.1.2. Extended Defects

Up to now we explored isolated defects in the bulk or different surface near sites. All cases can be characterized by narrow defect levels near the conduction band and core-level shifts smaller than 0.63 eV. Experimentally, peaks shifted by about 2 eV to lower binding energies are observed and associated with Ti^{3+} species [37]. To explore more configurations, we consider here one-dimensional extended defects, i.e., rows of oxygen vacancies in different crystallographic planes of $SrTiO_3$.

In Figure 3a the charge density resulting from a (010) oriented row of oxygen vacancies in a SrO plane is shown in the (100) plane. We chose a $1 \times 2 \times 4$ unit cell to separate the rows in a similar way as the bulk defects in the $2 \times 2 \times 4$ unit cell. In this plane, the defect states do not interact strongly as can be seen from the moderate broadening of the defect level in panel (b). Indeed, the Ti d_{z^2} states look very similar to the ones of isolated defects. The formation energy per unit cell of this extended defect is even 0.15 eV smaller than that of the isolated defect. Also, the shift of the $2p_{1/2}$ core level is very similar, 0.68 eV.

These findings are in sharp contrast to the properties of the (010) oriented defect row in the TiO_2 plane. Here, each Ti atom is nearest neighbor to two oxygen vacancies (V_O) and nominally corresponds to a Ti^{2+} species. Now a broad defect band forms in the band gap as can be seen from Figure 3d that is, in addition, spin-polarized. Note the one-dimensional character of the band with characteristic van-Hove singularities at both ends of the DOS. Also, in vacancy dimers with $V_O - Ti - V_O$ configurations a defect state splits off significantly from the conduction band both in the bulk [8] and near the surface [9]. The formation energy per $1 \times 2 \times 4$ unit cell is now 0.79 eV smaller than the bulk reference, a finding that is in-line with

the DFT+U results for vacancy dimers [8,9]. Similar effects are also found in rutile TiO_2 where linear vacancy clusters involving Ti^{2+} are very stable [12]. Looking at the $2p_{1/2}$ core-level shifts now large values of 2.41 eV (2.29 eV) for the majority (minority) states are found.

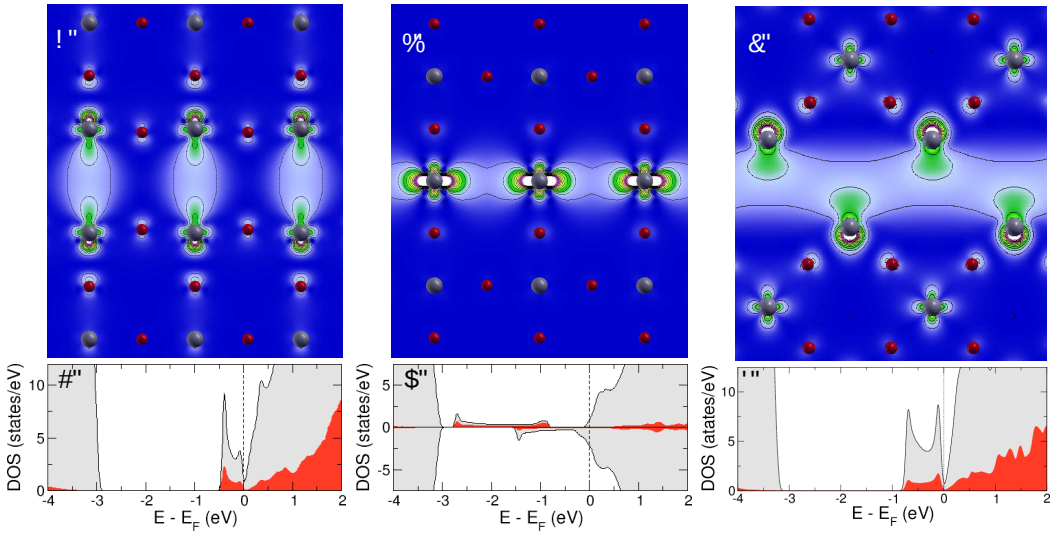

Figure 3. Electronic structure of aggregated oxygen vacancies in $SrTiO_3$: (**a**) Charge density of the vacancy-induced in-gap state of an oxygen vacancy row in an SrO plane. Red (gray) circles indicate oxygen (titanium) atoms. (**b**) Density of states (DOS) corresponding to panel (a): The local DOS of the Ti atoms next to the vacancies is shown in red, the total DOS in gray. (**c**) Like in (a), but now the vacancy row is situated in a TiO_2 plane. (**d**) Density of states (DOS) corresponding to panel (c): the color scheme follows panel (b), spin-up and spin-down DOS are shown by positive and negative values, respectively. (**e**) The oxygen vacancies are arranged in a (110) plane of $SrTiO_3$. The corresponding DOS is shown in panel (**f**).

Interestingly, this large core-level shift is not related to the presence of Ti with nominal charge +2, as can be seen from the calculation of the defect row in the (110) direction of $SrTiO_3$ shown in Figure 3e. Also, here we have a significant broadening of the defect level, but the core levels shift only 0.87 eV to higher binding energies. Although the nearest-neighbor distances from the vacancies to the Ti atoms are identical to the case of the TiO_2 (001) plane discussed above, the fact that the angle between $V_O -$ Ti $- V_O$ is now 90° instead of 180° is sufficient to lead to a completely different bonding situation. Also, in the case of vacancy dimers this configuration is energetically almost 0.8 eV less stable than the 180° configuration [8].

Comparing the three studied extended defects it can be seen that the defect levels are differently broadened to defect bands. A larger overlap of the wavefunctions along the defect row leads to increased bonding and to a larger bandwidth. In turn, the core-level shifts increase with the width of the defect band. This leads to peaks that are easier to resolve in core-level spectra, in particular if the defects occur in the vicinity of the probed surface.

2.2. Sr_2TiO_4

Finally, we investigated the electronic structure of Sr_2TiO_4 with oxygen vacancies. This is the first member of the Ruddlesden–Popper phases $Sr_{n+1}Ti_nO_{3n+1}$ that are formed by the insertion of SrO layers into the $SrTiO_3$ matrix. This process is energetically cheap [38] and often observed in the surface region of $SrTiO_3$ under oxidizing conditions [39]. It results in a stacking sequence of $TiO_2 -$ SrO $-$ SrO (001)

planes and it is thus also possible that techniques with certain surface sensitivity probe oxygen defects near SrO double planes. Again, as for defects in the SrO terminated $SrTiO_3$ surface, formally the nearest neighbor Ti atom has valence +2. Recently Sr_2TiO_4 was also discussed as material for resistive switching and measurements on Au/Sr_2TiO_4/Nb-doped $SrTiO_3$ junctions concluded that there is a clear correlation between resistive switching properties and the density of defects which work as fast migration paths for oxygen vacancies. Therefore, the control of the distribution and the density of defects is a major task in terms of the fabrication of reproducible and scalable resistive switching devices [40] and requires the characterization of defects in Sr_2TiO_4.

From Figure 4a it can be seen that again a narrow defect state forms at the bottom of the conduction band and although charge density plot in panel (b) suggest that the state is located at the nearest-neighbor Ti atom, the local density of state shows that most of the charge of this is actually located in the interstitial region between the atomic spheres. Since the charge accumulation at this Ti is small, also the $2p_{1/2}$ level shifts only by 0.46 eV towards higher binding energies. We further observe that the state remains localized within the first SrO layer and does not spread to the neighboring SrO layer due to a lack of available orbitals for hybridization. A similar effect was seen for Nb-doped $SrTiO_3$ where SrO − SrO layers form an insulating barrier for the *d*-states of Nb [41].

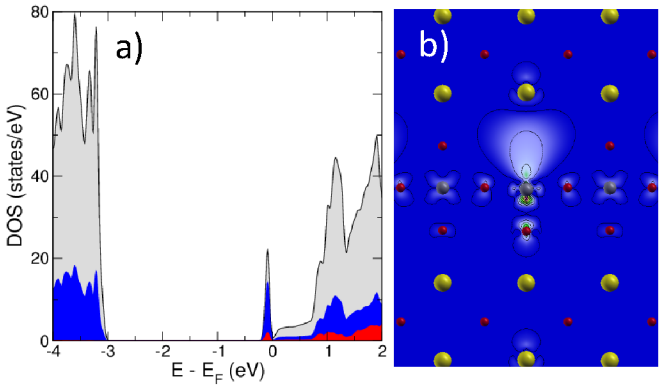

Figure 4. Electronic structure of oxygen vacancies in Sr_2TiO_4: (**a**) The local DOS of the Ti atoms next to the vacancies is shown in red, the total DOS in gray, the DOS located in the region between the atomic spheres (interstitial) is marked in blue. (**b**) Charge density of the vacancy-induced in-gap state of an oxygen vacancy row in an SrO plane. Sr atoms are indicated in yellow.

3. Discussion

Although it is believed that oxygen vacancies in insulating perovskites such as $SrTiO_3$ are decisive for the conductive properties observed in these materials, their characterization is far from trivial. Scanning-probe methods like scanning tunneling microscopy rely on the presence of states that reach the surface and provide conductive channels into the bulk. Due to the strongly anisotropic nature of the defect states, this is only fulfilled for certain configurations. Our calculations of near surface defects show that only defects in SrO planes will extend towards the (001) surface and those in TiO_2 planes might remain hidden due to the in-plane orientation of the defect states. Also, core-level spectroscopies, which are often used to identify Ti^{3+} or Ti^{2+} species in the Ti^{4+} matrix, allow no direct identification of the location or geometrical environment of the defect.

Most isolated defects that lead to nominally Ti^{3+} nearest-neighbor atoms induce only small core-level shifts in the Ti $2p_{1/2}$ states (0.4–0.6 eV) and even for some nominal Ti^{2+} atoms we find values in this range. An exception is the linear V_O− Ti − V_O configuration that produces states in the middle of the band gap or strongly dispersive bands in the case of an extended defect and core-level shifts of up to

2.4 eV. This peculiar arrangement is also energetically significantly more stable than other investigated extended defect structures and might be formed in regions of large defect densities. The observation of metallic conductivity in samples with low defect density [42] suggests that regions of locally enhanced deviation of stoichiometry exist in these crystals (Assuming a homogeneous, random distribution of isolated defects and taking the Mott criterion as guideline, about 4×10^{18} free charge carriers per cm^3 are necessary to initiate an insulator to metal transition. Assuming further that they are thermally activated from a shallow donor level, a rather high defect concentration is necessary (about $10^{20}/cm^3$ as observed in other perovskites [43])). Whether the simulated defect rows are a good model for the actual situation is difficult to decide by ab initio methods, but they feature signatures that are sometimes observed in conductive $SrTiO_3$ (like the strong core-level shifts [5]).

4. Methods

We use in our calculations the full-potential linearized augmented plane wave (FLAPW) method [44] as implemented in the FLEUR code [45]. We apply the generalized-gradient approximation (GGA) of Perdew, Burke and Ernzerhof [46], leading to a $SrTiO_3$ bulk lattice constant of 3.94 Å which is only 0.9% larger than the experimental lattice constant of 3.905 Å. GGA gives a good description of the structural parameters, but grossly underestimates the band gap. Unfortunately, for the calculation of defects such as an O-vacancy (V_O), this leads to unphysical results since these defect levels overlap with the conduction band and the wavefunctions are spread out over many unit cells [47]. A hybrid method based on the B3PW functional was applied in Ref. [21], giving a good lattice constant with a 0.3 eV overestimation of the band gap. Consequently, the neutral defect state is considerably split from the conduction band. As shown in Ref. [27], hybrid functionals such as HSE can give a good account of the structure and the band gap. Computationally, they are more costly than DFT+U methods which affects in particular the calculation of large supercells.

To give a similar correction of the band gap at moderate computational cost, we propose the DFT+U model [48], which both accounts for correlation effects on the Ti^{3+} sites and can be applied to open the band gap of the material. We apply a Hubbard-U not only on the d-shell of the Ti atoms, but also on the p electrons of the oxygen. If the U is applied to the Ti d-electrons only, the hybridization between these states and the O p electrons is weakened leading to an overestimation of the lattice constant and underestimation of the bulk modulus. A similar behavior was found in TiO_2 rutile [49]. Like in that reference, we use $U_d = 8$ eV ($J_d = 0.6$ eV) and $U_p = 6$ eV ($J_p = 0.1$ eV) here to get a good description of structural and electronic properties. The large U_d value is caused by the relatively small muffin-tin (MT) radius of Ti (1.9 Å) that is dictated by the large radius of O (1.7 Å) that must be used to localize a substantial fraction of the O p electrons in the MT where the DFT+U procedure is applied [50]. The charge density plots were produced using the xcrysden software [51].

Author Contributions: A.A.-Z. and G.B. performed the calculations, G.B. prepared the draft, A.A-Z., G.B., and S.B. discussed the results and contributed to the writing of the manuscript.

Funding: This research was funded by Deutsche Forschungsgemeinschaft within SFB 917 (Nanoswitches).

Acknowledgments: We gratefully acknowledge computing time at the JURECA supercomputer from the Jülich Supercomputing Centre.

Conflicts of Interest: The authors declare no conflict of interest.

References

1. Dearnaley, G.; Stoneham, A.M.; Morgan, D.V. Electrical phenomena in amorphous oxide films. *Rep. Prog. Phys.* **1970**, *33*, 1129. [CrossRef]
2. Beck, A.; Bednorz, J.G.; Gerber, C.; Rossel, C.; Widmer, D. Reproducible switching effect in thin oxide films for memory applications. *Appl. Phys. Lett.* **2000**, *77*, 139–141. [CrossRef]
3. Watanabe, Y.; Bednorz, J.G.; Bietsch, A.; Gerber, C.; Widmer, D.; Beck, A.; Wind, S.J. Current-driven insulator–conductor transition and nonvolatile memory in chromium-doped $SrTiO_3$ single crystals. *Appl. Phys. Lett.* **2001**, *78*, 3738–3740. [CrossRef]
4. Szot, K.; Speier, W.; Bihlmayer, G.; Waser, R. Switching the electrical resistance of individual dislocations in single crystalline $SrTiO_3$. *Nat. Mater.* **2006**, *5*, 312–320. [CrossRef]
5. Szot, K.; Bihlmayer, G.; Speier, W. Nature of the Resistive Switching Phenomena in TiO_2 and $SrTiO_3$: Origin of the Reversible Insulator-Metal Transition. *Solid State Phys.* **2014**, *65*, 353–559. [CrossRef]
6. Marrocchelli, D.; Sun, L.X.; Yildiz, B. Dislocations in $SrTiO_3$: Easy to reduce but not fast for oxygen transport. *J. Am. Chem. Soc.* **2015**, *137*, 4735–4748. [CrossRef]
7. Kwon, D.H.; Lee, S.; Kang, C.S.; Choi, Y.S.; Kang, S.J.; Cho, H.L.; Sohn, W.; Jo, J.; Lee, S.Y.; Oh, K.H.; et al. Unraveling the Origin and Mechanism of Nanofilament Formation in Polycrystalline $SrTiO_3$ Resistive Switching Memories. *Adv. Mater.* **2019**, *31*, 1901322. [CrossRef] [PubMed]
8. Cuong, D.D.; Lee, B.; Choi, K.M.; Ahn, H.S.; Han, S.; Lee, J. Oxygen Vacancy Clustering and Electron Localization in Oxygen-Deficient $SrTiO_3$: LDA + U Study. *Phys. Rev. Lett.* **2007**, *98*, 115503. [CrossRef] [PubMed]
9. Jeschke, H.O.; Shen, J.; Valentí, R. Localized versus itinerant states created by multiple oxygen vacancies in $SrTiO_3$. *New J. Phys.* **2015**, *17*, 023034. [CrossRef]
10. Anderson, J.S.; Hyde, H.G. On the possible role of dislocations in generating ordered and disordered shear structures. *J. Phys. Chem. Sol.* **1967**, *28*, 1393–1408. [CrossRef]
11. Bursill, L.A.; Hyde, H.G. Aggregation of Wadsley defrcts in slightly reduced rutile. *Philos. Mag.* **1971**, *23*, 3–15. [CrossRef]
12. Park, S.G.; Magyari-Kope, B.; Nishi, Y. Impact of Oxygen Vacancy Ordering on the Formation of a Conductive Filament in TiO_2 for Resistive Switching Memory. *IEEE Electron Device Lett.* **2011**, *32*, 197–199. [CrossRef]
13. Gao, P.; Ishikawa, R.; Feng, B.; Kumamoto, A.; Shibata, N.; Ikuhara, Y. Atomic-scale structure relaxation, chemistry and charge distribution of dislocation cores in $SrTiO_3$. *Ultramicroscopy* **2018**, *184*, 217–224. [CrossRef] [PubMed]
14. Rogala, M.; Bihlmayer, G.; Dabrowski, P.; Rodenbücher, C.; Wrana, D.; Krok, F.; Klusek, Z.; Szot, K. Self-reduction of the native TiO_2 (110) surface during cooling after thermal annealing-in-operando investigation. *Sci. Rep.* **2019**, *9*, 12563. [CrossRef] [PubMed]
15. Piskunov, S.; Heifets, E.; Eglitis, R.I.; Borstel, G. Bulk properties and electronic structure of $SrTiO_3$, $BaTiO_3$, $PbTiO_3$ perovskites: An ab initio HF/DFT study. *Comput. Mater. Sci.* **2004**, *29*, 165–178. [CrossRef]
16. Prosandeyev, S.A.; Fisenko, A.V.; Riabchinski, A.I.; Osipenko, I.A.; Raevski, I.P.; Safontseva, N. Study of intrinsic point defects in oxides of the perovskite family: I. Theory. *J. Phys. Condens. Matter* **1996**, *8*, 6705. [CrossRef]
17. King-Smith, R.D.; Vanderbilt, D. First-principles investigation of ferroelectricity in perovskite compounds. *Phys. Rev. B* **1994**, *49*, 5828. [CrossRef]
18. Ricci, D.; Bano, G.; Pacchioni, G. Electronic structure of a neutral oxygen vacancy in $SrTiO_3$. *Phys. Rev. B* **2003**, *68*, 224105. [CrossRef]
19. Evarestov, R.A.; Kotomin, E.A.; Zhukovskii, Y.F. DFT study of a single F center in cubic $SrTiO_3$ perovskite. *Int. J. Quantum Chem.* **2005**, *106*, 2173–2183. [CrossRef]
20. Carrasco, J.; Illas, F.; Lopez, N.; Kotomin, E.A.; Zhukovskii, Y.F.; Evarestov, R.A.; Mastrikov, Y.A.; Piskunov, S.; Maier, J. First-principles calculations of the atomic and electronic structure of F centers in the bulk and on the (001) surface of $SrTiO_3$. *Phys. Rev. B* **2006**, *73*, 064106. [CrossRef]
21. Kotomin, V.A.E.A.; Maier, J.; Evarestov, R.A. First-principles study of bulk and surface oxygen vacancies in $SrTiO_3$ crystal. *Eur. Phys. J. B* **2009**, *72*, 53. [CrossRef]

22. Astala, R.; Bristowe, P.D. Ab initio study of the oxygen vacancy in $SrTiO_3$. *Model. Simul. Mater. Sci. Eng.* **2001**, *9*, 415. [CrossRef]
23. Samanta, A.; Weinan, E.; Zhang, S.B. Method for defect stability diagram from ab initio calculations: A case study of $SrTiO_3$. *Phys. Rev. B* **2012**, *86*, 195107. [CrossRef]
24. Lin, C.; Mitra, C.; Demkov, A.A. Orbital ordering under reduced symmetry in transition metal perovskites: Oxygen vacancy in $SrTiO_3$. *Phys. Rev. B* **2012**, *86*, 161102. [CrossRef]
25. Lin, C.; Demkov, A.A. Electron Correlation in Oxygen Vacancy in $SrTiO_3$. *Phys. Rev. Lett.* **2013**, *111*, 217601. [CrossRef]
26. Hao, X.; Wang, Z.; Schmid, M.; Diebold, U.; Franchini, C. Coexistence of trapped and free excess electrons in $SrTiO_3$. *Phys. Rev. B* **2015**, *91*, 085204. [CrossRef]
27. Janotti, A.; Varley, J.B.; Choi, M.; Van de Walle, C.G. Vacancies and small polarons in $SrTiO_3$. *Phys. Rev. B* **2014**, *90*, 085202. [CrossRef]
28. Hou, Z.; Terakura, K. Defect States Induced by Oxygen Vacancies in Cubic $SrTiO_3$: First-Principles Calculations. *J. Phys. Soc. Jpn.* **2010**, *79*, 114704. [CrossRef]
29. Graetz, J.; Reilly, J.J.; Johnson, J.; Ignatov, A.Y.; Tyson, T.A. X-ray absorption study of Ti-activated sodium aluminum hydride. *Appl. Phys. Lett.* **2004**, *85*, 500–502. [CrossRef]
30. Drera, G.; Salvinelli, G.; Brinkman, A.; Huijben, M.; Koster, G.; Hilgenkamp, H.; Rijnders, G.; Visentin, D.; Sangaletti, L. Band offsets and density of Ti^{3+} states probed by X-ray photoemission on $LaAlO_3/SrTiO_3$ heterointerfaces and their $LaAlO_3$ and $SrTiO_3$ bulk precursors. *Phys. Rev. B* **2013**, *87*, 075435. [CrossRef]
31. Sitaputra, W.; Sivadas, N.; Skowronski, M.; Xiao, D.; Feenstra, R.M. Oxygen vacancies on SrO-terminated $SrTiO_3(001)$ surfaces studied by scanning tunneling spectroscopy. *Phys. Rev. B* **2015**, *91*, 205408. [CrossRef]
32. Tanaka, H.; Matsumoto, T.; Kawai, T.; Kawai, S. Surface Structure and Electronic Property of Reduced $SrTiO_3$ (100) Surface Observed by Scanning Tunneling Microscopy/Spectroscopy. *Jpn. J. Appl. Phys.* **1993**, *32*, 1405. [CrossRef]
33. Fang, Z.; Terakura, K. Spin and orbital polarizations around oxygen vacancies on the (001) surfaces of $SrTiO_3$. *Surf. Sci.* **2000**, *470*, L75. [CrossRef]
34. Shen, J.; Lee, H.; Valentí, R.; Jeschke, H.O. Ab initio study of the two-dimensional metallic state at the surface of $SrTiO_3$: Importance of oxygen vacancies. *Phys. Rev. B* **2012**, *86*, 195119. [CrossRef]
35. Li, Z.Q.; Zhu, J.L.; Wu, C.Q.; Tang, Z.; Kawazoe, Y. Relaxations of TiO_2- and SrO-terminated $SrTiO_3$ (001) surfaces. *Phys. Rev. B* **1998**, *58*, 8075–8078. [CrossRef]
36. Shiraki, I.; Miki, K. $SrTiO_3$ (100) $\sqrt{5} \times \sqrt{5} - R26.6$ surface observed by high-resolution scanning tunneling microscopy. *Surf. Sci.* **2011**, *605*, 1304–1307. [CrossRef]
37. Walker, S.M.; Bruno, F.Y.; Wang, Z.; de la Torre, A.; Riccó, S.; Tamai, A.; Kim, T.K.; Hoesch, M.; Shi, M.; Bahramy, M.S.; et al. Carrier-Density Control of the $SrTiO_3$ (001) Surface 2D Electron Gas studied by ARPES. *Adv. Mater.* **2015**, *27*, 3894–3899. [CrossRef]
38. Noguera, C. Theoretical investigation of the Ruddlesden-Popper compunds $Sr_{n+1}Ti_nO_{3n+1}$ (n = 1–3). *Philos. Mag. Lett.* **2000**, *80*, 173. [CrossRef]
39. Szot, K.; Speier, W.; Herion, J.; Feiburg, C. Restructuring of the surface region in $SrTiO_3$. *Appl. Phys. A* **1996**, *64*, 55. [CrossRef]
40. Shibuya, K.; Dittmann, R.; Mi, S.; Waser, R. Impact of Defect Distribution on Resistive Switching Characteristics of Sr_2TiO_4 Thin Films. *Adv. Mater.* **2010**, *22*, 411–414. [CrossRef]
41. Rodenbücher, C.; Speier, W.; Bihlmayer, G.; Breuer, U.; Waser, R.; Szot, K. Cluster-like resistive switching of $SrTiO_3$:Nb surface layers. *New J. Phys.* **2013**, *15*, 103017. [CrossRef]
42. Lee, C.; Yahia, J.; Brebner, J.L. Electronic Conduction in Slightly Reduced Strontium Titanate at Low Temperatures. *Phys. Rev. B* **1971**, *3*, 2525–2533. [CrossRef]
43. Kolodiazhnyi, T. Insulator-metal transition and anomalous sign reversal of the dominant charge carriers in perovskite $BaTiO_{3-\delta}$. *Phys. Rev. B* **2008**, *78*, 045107. [CrossRef]

44. Wimmer, E.; Krakauer, H.; Weinert, M.; Freeman, A.J. Full-potential self-consistent linearized-augmented-plane-wave method for calculating the electronic structure of molecules and surfaces: O_2 molecule. *Phys. Rev. B* **1981**, *24*, 864. [CrossRef]
45. The Jülich Full-Linearized Augmented Plane Waves (FLAPW) Code Family. Available online: http://www.flapw.de (accessed on 18 October 2019).
46. Perdew, J.P.; Burke, K.; Ernzerhof, M. Generalized Gradient Approximation Made Simple. *Phys. Rev. Lett.* **1996**, *77*, 3865. [CrossRef]
47. Carrasco, J.; Illas, F.; Lopez, N.; Kotomin, E.A.; Zhukovskii, Y.F.; Piskunov, S.; Maier, J.; Hermansson, K. First principles simulations of F centers in cubic $SrTiO_3$. *Phys. Status Solidi C* **2005**, *2*, 153–158. [CrossRef]
48. Solovyev, I.V.; Dederichs, P.H.; Anisimov, V.I. Corrected atomic limit in the local-density approximation and the electronic structure of *d* impurities in Rb. *Phys. Rev. B* **1994**, *50*, 16861. [CrossRef]
49. Park, S.G.; Magyari-Köpe, B.; Nishi, Y. Electronic correlation effects in reduced rutile TiO_2 within the LDA + *U* method. *Phys. Rev. B* **2010**, *82*, 115109. [CrossRef]
50. Shick, A.B.; Liechtenstein, A.I.; Pickett, W.E. Implementation of the LDA+U method using the full-potential linearized augmented plane-wave basis. *Phys. Rev. B* **1999**, *60*, 10763–10769. [CrossRef]
51. Kokalj, A. Computer graphics and graphical user interfaces as tools in simulations of matter at the atomic scale. *Comput. Mater. Sci.* **2003**, *28*, 155–168. [CrossRef]